ELSEVIER

Physica A 261 (1998) 391–408

PHYSICA A

Electrostatic spectrum of renormalized polarizability for nonpolar dielectric

Piotr Szymczak *, Bogdan Cichocki

Institute of Theoretical Physics, Warsaw University, Hoża 69, 00-618 Warsaw, Poland

Received 10 February 1998; received in revised form 9 April 1998

Abstract

The Drude–Lorentz model of a nonpolar dielectric with the simple cubic, face-centered and body-centered crystal lattice structures is considered. The electrostatic spectral density of the renormalized polarizability is found. The problem is equivalent to the calculation of the electronic density of states in the model. The obtained spectra are analyzed and the critical points are identified. The results are compared with the computer simulation data for a hard-sphere fluid. In the latter, the structure analogous to the transverse and longitudinal polarization modes characteristic for a solid dielectric is shown to exist.

PACS: 05.90.+m; 41.20.Cv; 71.38.+i; 71.45.Gm
Keywords: Drude–Lorentz model; Density of states; Renormalized polarizability; Electrostatic spectrum

1. Introduction

The classical Drude–Lorentz model [1] is a system of harmonic oscillators coupled via electrostatic dipole–dipole interactions. The model captures the key features of the dielectric response of nonpolar fluids and, therefore, was and still is a subject of extensive theoretical studies.

There are two basic problems posed for nonpolar systems. The first one is to determine the complex dielectric constant; its imaginary part gives the absorption spectrum. The second problem is to find the so-called renormalized (or effective) polarizability which characterizes the Onsager's [2,3] reaction field. This field is due to the

* Corresponding author.

0378-4371/98/$ – see front matter
PII: S0378-4371(98)00266-0

polarization of the medium induced by a selected frozen dipole. The dependence of the renormalized polarizability on the bare polarizability of atoms leads to a spectral representation with the spectral density which is closely related to the density of states in the Drude–Lorentz model [3–5]. This is also relevant for the van der Waals binding energy of the fluid [6].

The absorption spectrum and the density of states have been determined by computer simulations for a fluid with hard sphere statistics [3,7], as well as for Lennard–Jones fluids [8]. There exists also a theoretical explanation of the simulation results in the case of very low-density systems. It has been shown, for example, that the spectra have nontrivial universal shapes in the dilute gas limit [8–11], universal in the sense that details of the geometrical microstructure are irrelevant. However, for higher densities, even in the semi-diluted regime, theoretical approximation schemes are not fully satisfactory. The main discrepancy is that the renormalized polarizability spectrum determined by simulations consists of two very broad peaks, while present theoretical calculations lead to one broad peak structure.

In this paper we will show that these two broad peaks correspond to contributions from the longitudinal and transverse polarizability modes characteristic for crystals. To do that we calculate the renormalized polarizability spectrum for the primitive cubic lattices and determine the separate contributions from different polarization modes. In this case one can use the solid state physics methods and get very accurate results. It is worth mentioning that for the lattices the effective dielectric constant satisfies the Clausius–Mossotti formula exactly.

Having very accurate results for the cubic lattices, we will also check the quality of the continued fraction method used by Cichocki and Felderhof [3,7] to determine the spectra in disordered systems. In this method it is only necessary to calculate a few first moments of the spectral density. The rest follows from the powerful theory of Stieltjes integrals [12,13].

2. Drude–Lorentz model of a nonpolar dielectric

We consider the Drude–Lorentz model of a nonpolar dielectric. In this model each molecule is represented as a fixed nucleus accompanied by an elastically bounded "dispersion electron" with the eigenfrequency ω_0. The interaction potential between any two molecules is limited to dipole–dipole terms. The Hamiltonian for such a system reads

$$H = \sum_i \frac{\mathbf{p}_i^2}{2m} + \sum_i \frac{1}{2} m\omega_0^2 \mathbf{u}_i^2 - \frac{1}{2} e^2 \sum_{i,j} \mathbf{u}_i \cdot \hat{T}_{ij} \cdot \mathbf{u}_j \,, \tag{1}$$

where $\mathbf{u}_i$ is the deviation of the ith electron from its equilibrium position, $\mathbf{p}_i$ its momentum and $\hat{T}_{ij}$ is the dipole–dipole interaction tensor

$$\hat{T}_{ij} = \hat{T}(\mathbf{r}_i - \mathbf{r}_j),$$

Table 1
The characteristics of the primitive cubic lattices considered in the paper

Lattice	Basis vectors	Elementary cell volumne (v)	Nearest neighbour distance	Reciprocal lattice basis
sc	(1,0,0)			$2\pi(1,0,0)$
	(0,1,0)	1	1	$2\pi(0,1,0)$
	(0,0,1)			$2\pi(0,0,1)$
fcc	(0,1,1)			$\pi(-1,1,1)$
	(1,0,1)	2	$\frac{\sqrt{2}}{2}$	$\pi(1,-1,1)$
	(1,1,0)			$\pi(1,1,1)$
bcc	$(-1,1,1)$			$\pi(0,1,1)$
	$(1,-1,1)$	4	$\frac{\sqrt{3}}{2}$	$\pi(1,0,1)$
	$(1,1,-1)$			$\pi(1,1,0)$

where

$$\hat{T}(\mathbf{r}) = \frac{-\hat{I} + 3\hat{\mathbf{r}}\hat{\mathbf{r}}}{r^3} \,. \tag{2}$$

Suppose that the dielectric has a crystal structure with the unit cell specified by the basic vectors $\mathbf{a}_1, \mathbf{a}_2, \mathbf{a}_3$. The lattice vector is

$$\mathbf{r}_\mathbf{n} = n_1\mathbf{a}_1 + n_2\mathbf{a}_2 + n_3\mathbf{a}_3 \,, \tag{3}$$

where $\mathbf{n}$ denotes the set of integers (n_1, n_2, n_3). Here we will consider the three primitive cubic lattices only: fcc, bcc and sc. Nevertheless, our calculations are automatically applicable to any other lattice structure. The parameters of the lattices considered in the paper are given in Table 1 (note that all the distances are scaled here by the lattice constant).

Let us now rewrite the Hamiltonian (1) in the reciprocal space variables

$$\mathbf{u}(\mathbf{k}) = \sqrt{\frac{v}{(2\pi)^3}} \sum_\mathbf{n} \mathbf{u}_\mathbf{n} e^{-i\mathbf{k}\cdot\mathbf{r}_\mathbf{n}} \,, \tag{4}$$

and

$$\mathbf{p}(\mathbf{k}) = \sqrt{\frac{v}{(2\pi)^3}} \sum_\mathbf{n} \mathbf{p}_\mathbf{n} e^{i\mathbf{k}\cdot\mathbf{r}_\mathbf{n}} \,, \tag{5}$$

where the summation is over the lattice points and v is the elementary cell volume. In terms of these variables the Hamiltonian reads

$$H = \int_{BZ} \frac{\mathbf{p}^{\star}(\mathbf{k})\cdot\mathbf{p}(\mathbf{k})}{2m}\, d\mathbf{k} + \int_{BZ} \frac{1}{2} m\omega_0^2 \mathbf{u}^{\star}(\mathbf{k})\cdot\mathbf{u}(\mathbf{k})\, d\mathbf{k} - \frac{1}{2} e^2 \int_{BZ} \mathbf{u}^{\star}(\mathbf{k})\cdot\hat{T}(\mathbf{k})\cdot\mathbf{u}(\mathbf{k})\, d\mathbf{k}\,, \tag{6}$$

where the integrals are performed over the Brillouin zone, and $\hat{T}(\mathbf{k})$ is the Fourier transform of the dipole–dipole interaction tensor

$$\hat{T}(\mathbf{k}) = \sum_{\mathbf{n}}{}' \hat{T}(\mathbf{r_n}) e^{i\mathbf{k}\cdot\mathbf{r_n}}\,. \tag{7}$$

Prime means that $\mathbf{n}=0$ is excluded from the summation.

Since the above Hamiltonian is quadratic in $\mathbf{u}(\mathbf{k})$, we are able to express any solution of the equation of motion in terms of the normal modes (polarization waves) [14] of the form

$$\mathbf{u_n} = \mathbf{A}(\mathbf{k}) e^{i[\mathbf{k}\cdot\mathbf{r_n} - \omega(\mathbf{k})t]}\,, \tag{8}$$

with three mutually orthogonal polarizations for each $\mathbf{k}$. The frequencies $\omega_i(\mathbf{k})$ of the modes are given by

$$\omega_i(\mathbf{k}) = \sqrt{\omega_0^2 - \frac{e^2}{m}\lambda_i(\mathbf{k})} = \omega_0\sqrt{1-\alpha_0\lambda_i(\mathbf{k})}, \quad i=1,2,3 \tag{9}$$

where $\alpha_0 = e^2/m\omega_0^2$ is a static polarizability in the Drude–Lorentz model and $\lambda_i(\mathbf{k})$ are eigenvalues of the operator $\hat{T}(\mathbf{k})$.

We see that these eigenvalues are connected with the frequencies of collective oscillations of Drude–Lorentz oscillators. The eigenvectors give directions of vibrations. In particular, one can show that in the long-wave limit ($\mathbf{k}\to 0$) the three polarization waves described above reduce to one longitudinal and two degenerate transverse waves with the frequencies

$$\omega_L = \omega_0\sqrt{1+\frac{8\pi\alpha_0}{3v}}, \qquad \omega_T = \omega_0\sqrt{1-\frac{4\pi\alpha_0}{3v}}\,. \tag{10}$$

One can now define the density of states $\rho_D(\omega)$ in the Drude–Lorentz model [3–5]; $\rho_D(\omega)\,d\omega$ is a number of the polarization waves with frequencies between ω and $\omega + d\omega$.

The density of states $\rho_D(\omega)$ is closely connected with the so-called electrostatic spectrum density. To define this quantity, let us consider a crystal lattice of polarizable point dipoles with polarizability α. Next, apply a uniform electric field $\mathbf{E}_0$ locally on one of the lattice sites. The electric dipole moment induced in this site will in turn

induce dipole moments in other sites and so on. As a result of these interactions dipoles are induced in each lattice point. They are determined by the system of equations

$$\boldsymbol{\mu}_j = \alpha \left[\mathbf{E}_0 \delta_{j1} + \sum_{k \neq j} \hat{T}_{jk} \cdot \boldsymbol{\mu}_k \right], \quad j = 1, 2, \ldots . \tag{11}$$

Here we use an index "1" for the selected site where $\mathbf{E}_0$ is applied.

The renormalized polarizability α' is defined by the relation

$$\boldsymbol{\mu}_1 = \alpha' \cdot \mathbf{E}_0 . \tag{12}$$

Due to the lattice symmetry α' is a scalar. The product of the number density n (for crystals $n = 1/v$) and the renormalized polarizability α' defines the so-called self-susceptibility. The coefficient α' is a very important characteristic of a nonpolar dielectric and is related to Onsager's [2,3] reaction field $\mathbf{R}$ by

$$\mathbf{R} = \left(\frac{\alpha'}{\alpha} - 1 \right) \mathbf{E}_0 . \tag{13}$$

To find a microscopic expression for α', let us introduce infinite-dimensional vectors $\boldsymbol{\mu} = (\boldsymbol{\mu}_1, \boldsymbol{\mu}_2, \ldots)$ and $\mathbf{E} = (\mathbf{E}_0, 0, 0, 0 \ldots)$ and the infinite matrix

$$\mathscr{T} = \begin{pmatrix} 0 & \hat{T}_{12} & \hat{T}_{13} & \ldots \\ \hat{T}_{21} & 0 & \hat{T}_{23} & \ldots \\ \hat{T}_{31} & \hat{T}_{32} & 0 & \ldots \\ \vdots & \vdots & \vdots & \vdots \end{pmatrix} .$$

We can now rewrite Eq. (11) in the following form:

$$\boldsymbol{\mu} = \alpha(\mathbf{E} + \mathscr{T} \cdot \boldsymbol{\mu}) . \tag{14}$$

Therefore,

$$\boldsymbol{\mu} = \frac{1}{z - \mathscr{T}} \mathbf{E} , \tag{15}$$

where $z = 1/\alpha$. Thus, we get the following expression for the renormalized polarizability:

$$\alpha' = \frac{1}{3} \sum_{\beta} \left\langle \mathbf{e}_{1\beta} \left| \frac{1}{z - \mathscr{T}} \right| \mathbf{e}_{1\beta} \right\rangle , \tag{16}$$

where $\mathbf{e}_{1\beta} = (\mathbf{e}_\beta, 0, 0, 0 \ldots)$ and $\mathbf{e}_\beta$ is a Cartesian unit vector for the direction $\beta = x, y, z$.

Next, let us consider the eigenproblem for the matrix $\mathscr{T}$

$$\mathscr{T} \, |v\gamma\rangle = v \, |v\gamma\rangle , \tag{17}$$

where $|v\gamma\rangle$ is the eigenvector corresponding to the eigenvalue v (γ accounts for the possible degeneracy). The eigenvalues v are real since the matrix $\mathscr{T}$ is real and symmetric.

With the completeness relation

$$\sum_{\gamma} \int_{-\infty}^{\infty} |v\gamma\rangle \langle v\gamma| \, dv = \hat{I} \,, \tag{18}$$

one has

$$\frac{1}{z-\mathscr{T}} = \sum_{\gamma} \int_{-\infty}^{\infty} \frac{|v\gamma\rangle \langle v\gamma|}{z-v} \, dv \,. \tag{19}$$

This allows to write the renormalized polarizability in the following way:

$$\alpha' = \frac{1}{3} \sum_{\beta} \sum_{\gamma} \int_{-\infty}^{\infty} \frac{|\langle \mathbf{e}_{1\beta}|v\gamma\rangle|^2}{z-v} \, dv \,, \tag{20}$$

Let us define now the positive real function

$$\rho(v) \equiv \frac{1}{3} \sum_{\beta} \sum_{\gamma} |\langle \mathbf{e}_{1\beta}|v\gamma\rangle|^2 \,, \tag{21}$$

which due to the relation (18) is normalized to unity

$$\int_{-\infty}^{\infty} \rho(v) \, dv = 1 \,. \tag{22}$$

One can rewrite Eq. (20) in the form

$$\alpha'(z) = \int_{-\infty}^{\infty} \frac{\rho(v)}{z-v} \, dv \,. \tag{23}$$

The above relation is called the spectral representation of the renormalized polarizability. The spectral density $\rho(v)$ is sometimes called "electrostatic spectrum" of α'. By the arguments analogous to those presented in [3,7], one can show that the spectral density $\rho(v)$ is nonzero only in the finite interval of real axis. The relation

$$\lim_{\eta \to 0} \frac{1}{z-v-\eta i} = P\left(\frac{1}{z-v}\right) + i\pi\delta(z-v) \,, \tag{24}$$

also leads to

$$\rho(v) = \lim_{\eta \to 0} \frac{1}{\pi} \operatorname{Im} \alpha'(v - i\eta) \,. \tag{25}$$

It has been shown in Ref. [10] (see also the next section) that the spectral density ρ is related to the density of states ρ_D in the Drude–Lorentz model in the following way:

$$\rho_D(\omega) = \frac{2m\omega}{e^2} \rho\left(v = \frac{m}{e^2}(\omega_0^2 - \omega^2)\right) . \tag{26}$$

Thus to find the effect of broadening due to the dipole interactions on the density of states it is enough to analyze the simple electrostatic system described above.

3. Reciprocal space formulation of the problem

Our aim is to calculate the spectral density ρ for the cubic lattices. To proceed we will derive an expression for the renormalized polarizability in terms of reciprocal space integrals. First, we expand this polarizability in the inverse powers of z. Eq. (16) leads to

$$\begin{aligned}\alpha'(z) &= \frac{1}{3}\sum_{\beta}\left\langle \mathbf{e}_{1\beta}|z^{-1}+\mathscr{T}z^{-2}+\mathscr{T}^2z^{-3}+\cdots|\mathbf{e}_{1\beta}\right\rangle \\ &= \frac{1}{3}\mathrm{Tr}\left(z^{-1}\left[1+z^{-2}\sum_{l}\hat{T}_{1l}\hat{T}_{l1}+z^{-3}\sum_{lm}\hat{T}_{1l}\hat{T}_{lm}\hat{T}_{m1}+\cdots\right]\right), \end{aligned} \tag{27}$$

where Tr stands for the trace over Cartesian indices – (x,y,z) and we have used the fact that the operator $\hat{T}$ is traceless. The relation

$$\int_{BZ} e^{i\mathbf{k}\cdot\mathbf{r}}\,d\mathbf{k} = \frac{8\pi^3}{v}\sum_{\mathbf{n}}\delta_{\mathbf{r},\mathbf{r}_\mathbf{n}}\,, \tag{28}$$

allows us to express the successive terms in Eq. (27) as

$$\sum_{a_1,a_2,\ldots,a_j}\hat{T}_{1a_1}\hat{T}_{a_1a_2}\ldots\hat{T}_{a_j1} = \frac{v}{8\pi^3}\int_{BZ}\hat{T}^{j+1}(\mathbf{k})\,d\mathbf{k}\,. \tag{29}$$

Taking into account that

$$\mathrm{Tr}(\hat{T}^j(\mathbf{k})) = \sum_{i=1}^{3}\lambda_i^j(\mathbf{k})\,,$$

with $\lambda_i(\mathbf{k})$ being eigenvalues of $\hat{T}(\mathbf{k})$, one can write

$$\alpha'(z) = \frac{v}{24\pi^3}\sum_{i=1}^{3}\sum_{j=0}^{\infty}\int_{BZ}\lambda_i^j(\mathbf{k})z^{-j-1}\,d\mathbf{k}\,. \tag{30}$$

Finally, performing the sum over j, one gets

$$\alpha'(z) = \frac{v}{24\pi^3}\sum_{i=1}^{3}\int_{BZ}\frac{d\mathbf{k}}{z-\lambda_i(\mathbf{k})}\,, \tag{31}$$

and the spectral density becomes

$$\rho(v) = \lim_{\eta\to 0}\frac{v}{24\pi^4}\,\mathrm{Im}\left(\sum_{i=1}^{3}\int_{BZ}\frac{1}{v-\lambda_i(\mathbf{k})-i\eta}\,d\mathbf{k}\right). \tag{32}$$

Therefore, we have reduced a problem of finding the spectral density to performing the Fourier transform of the dipole–dipole interaction tensor $\hat{T}(\mathbf{k})$, solving its eigenproblem and carrying out the integral (32) over the Brillouin zone.

From Eq. (32) we see that $\rho(\lambda)\,d\lambda$ can be interpreted as a number of eigenvalues of a tensor $\hat{T}(\mathbf{k})$ belonging to the interval $(\lambda, \lambda + d\lambda)$. This remark, together with the formula (9), leads immediately to the relation (26) between the electrostatic spectrum and the Drude–Lorentz density of states.

The sum (7) can be calculated using the method described by Nijboer and de Wette [16] based on the Ewald summation procedure. After simple modifications of their results we get

$$\hat{T}(\mathbf{k}) = \frac{4}{3\sqrt{\pi}} {\sum_{\mathbf{n}}}' \Gamma\left(\frac{5}{2}, \tau\pi r_{\mathbf{n}}^2\right) \frac{-\hat{I} + 3\hat{\mathbf{r}}_{\mathbf{n}}\hat{\mathbf{r}}_{\mathbf{n}}}{r_{\mathbf{n}}^3} e^{i\mathbf{k}\cdot\mathbf{r}_{\mathbf{n}}} - \frac{4\pi}{3v} \sum_{\mathbf{n}} e^{-\frac{\pi q_{\mathbf{n}}^2}{\tau}} (-\hat{I} + 3\hat{\mathbf{q}}_{\mathbf{n}}\hat{\mathbf{q}}_{\mathbf{n}}) \,. \tag{33}$$

where $\mathbf{q}_{\mathbf{n}} = \mathbf{k} - \mathbf{h}_{\mathbf{n}}$ with $\mathbf{h}_{\mathbf{n}}$ being the reciprocal lattice vectors and τ – the so-called Ewald parameter that should be chosen appropriately to obtain equally rapid convergence in the direct and reciprocal sums. Formula (33) is fast convergent. In practice, to calculate $\hat{T}(\mathbf{k})$ with the accuracy of the order of 10^{-7} it is enough to sum over 4^3 lattice points.

It is not necessary to evaluate $\hat{T}(\mathbf{k})$ for all $\mathbf{k} \in BZ$ since the following relations hold:

$$\hat{T}(k_x, k_y, k_z) = \hat{T}(\sigma(k_x, k_y, k_z)) \,, \tag{34}$$

where k_x, k_y, k_z are the Cartesian components of $\mathbf{k}$ and $\sigma(k_x, k_y, k_z)$ denotes any permutation of (k_x, k_y, k_z). Moreover,

$$\hat{T}(\varepsilon_1 k_x, \varepsilon_2 k_y, \varepsilon_3 k_z) = \begin{pmatrix} \varepsilon_1 & & \\ & \varepsilon_2 & \\ & & \varepsilon_3 \end{pmatrix} \hat{T}(k_x, k_y, k_z) \begin{pmatrix} \varepsilon_1 & & \\ & \varepsilon_2 & \\ & & \varepsilon_3 \end{pmatrix} , \tag{35}$$

where $\varepsilon_i = \pm 1$. Thus we need to evaluate $\hat{T}(\mathbf{k})$ only for $\mathbf{k}$ obeying

$$0 \leqslant k_z \leqslant k_y \leqslant k_x \,. \tag{36}$$

Together with the observation that $\mathbf{k}$ should remain in the first Brillouin zone of the reciprocal lattice, the above finally imposes the following conditions on $\mathbf{k}$:

- for sc

$$0 \leqslant k_z \leqslant k_y \leqslant k_x \leqslant \pi \,, \tag{37}$$

- for fcc

$$\begin{aligned} &0 \leqslant k_z \leqslant k_y \leqslant k_x \leqslant \pi \\ &k_x + k_y + k_z \leqslant \tfrac{3}{2}\pi \,, \end{aligned} \tag{38}$$

- for bcc

$$0 \leqslant k_z \leqslant k_y \leqslant k_x \leqslant \pi$$
$$k_x + k_y \leqslant \pi \,. \tag{39}$$

The relations (37)–(39) describe the so-called Irreducible Brillouin Zones (IBZ) for the respective lattices.

4. Calculation of the spectral density

There exist numerous methods of computing the integrals of the form Eq. (32) – they often arise in frequency distribution function calculations. Different methods of dealing with such integrals are described at length in the review article by Gilat [17]. Here we use two of the standard methods described in [17]. The first is the RS ("root sampling") method in which one solves the $\hat{T}(\mathbf{k})$ eigenproblem for $\mathbf{k}$ vectors forming a fine uniform mesh in the irreducible section of the first Brillouin zone. Then the obtained eigenvalues are sorted out into a number of channels thereby forming a histogram which approximates the spectrum.

The second method is the LA ("linear analytic") method in which one computes the eigenvalues $\lambda_i(\mathbf{k})$, as well as their gradients $\nabla\lambda_i(\mathbf{k})$, at evenly spaced points in reciprocal space and then finds λ in between by means of a linear extrapolation.

In addition, we use the continued fraction (CF) method. We proceed in the analogous way to that described in Refs. [7,3] where the CF method was applied to calculate the electrostatic spectrum for the dielectric constant and the renormalized polarizability in fluids. In such systems, because of the lack of periodicity, one cannot apply standard solid-state methods using the reciprocal-space formulation. The idea of the CF method is to represent $\alpha'(z)$ by a continued fraction of the form

$$\alpha'(z) = \cfrac{a_0}{z + b_1 - \cfrac{a_1}{z+b_2 - \cfrac{a_2}{z+b_3-\ldots}}} \,, \tag{40}$$

where a_i and b_i are real and $a_i > 0$ (the so-called real J-fraction [12]).

The possibility of finding continued fraction representation for $\alpha'(z)$ is ensured by the theorem due to Markoff [13]. It states that every function of the form (23), with the normalized positive spectral density ρ, can be represented as a real J-fraction. Moreover, if we know the coefficients c_n in the asymptotic series

$$\alpha'(z) = \sum_{n=0}^{\infty} \frac{c_n}{z^{n+1}} \,, \tag{41}$$

then we can calculate a_i and b_i by means of a simple and fast algorithm described in Ref. [12]. The coefficients c_n are the moments of the spectral density and can be

Table 2
List of the first ten moments c_n defined by Eq. (42) for the three primitive cubic lattices

n	sc	fcc	bcc
0	1	1	1
1	0	0	0
2	16.803	3.6138	0.9076
3	39.705	5.0854	0.6324
4	606.42	26.031	1.6487
5	3135.6	69.551	2.1595
6	31088	266.98	4.1688
7	2.1819×10^5	879.58	6.7646
8	1.9229×10^6	3219.6	12.357
9	1.5256×10^7	11430	21.732
10	1.3123×10^8	42006	39.786

expressed in our case as

$$c_n = \int_{-\infty}^{\infty} \rho(v) v^n \, dv = \frac{\upsilon}{24\pi^3} \sum_{i=1}^{3} \int_{BZ} \lambda_i^n(\mathbf{k}) \, d\mathbf{k} \, . \tag{42}$$

Due to the normalization condition (22) $c_0 = 1$ and since the operator $\hat{T}(\mathbf{k})$ is traceless, $c_1 = 0$.

The integrals in formula (42) are much easier to carry out than the integral (32) and can be performed with high accuracy. In Table 2 we list the values of the first ten moments c_n. From that we have found the coefficients a_i and b_i of the representation (40). Their values are given in the Table 3.

The results suggest that a_i and b_i quite quickly tend to the limiting values a_∞ and b_∞. If we replace the coefficients a_i and b_i from a certain level onward by a_∞ and b_∞, respectively, then we obtain

$$\alpha'(z) = \cfrac{a_1}{z + b_1 - \cfrac{a_2}{z + b_2 + \cdots - \cfrac{a_{n-1}}{z + b_{n-1} - P}}} \, , \tag{43}$$

with P obeying

$$P = \frac{a_\infty}{b_\infty + z - P} \, . \tag{44}$$

So that

$$P = \tfrac{1}{2}(z + b_\infty) + \tfrac{1}{2}\sqrt{(z + b_\infty)^2 - 4a_\infty} \, , \tag{45}$$

where one must take the branch of the square root with a cut between $z_1 = 2\sqrt{a_\infty} - b_\infty$ and $z_2 = -2\sqrt{a_\infty} - b_\infty$. In this way, we get an analytical (although approximate) expression for $\alpha'(z)$ and consequently, by use of Eq. (25), for $\rho(v)$. It is worth mentioning

Table 3
Coefficients a_n i b_n in the continued fraction representation (40) of the renormalized polarizability for the three primitive cubic lattices. Due to the normalization a_0 is equal to unity

	sc		fcc		bcc	
n	a_n	b_n	a_n	b_n	a_n	b_n
1	16.803	0	3.6138	0	0.9076	0
2	13.703	2.3628	1.6111	1.4076	0.4234	0.6968
3	12.894	2.1344	2.9642	1.0900	0.7225	0.4396
4	13.880	2.3341	2.1037	0.9018	0.5378	0.5643
5	14.399	2.1104	2.7708	1.1675	0.6806	0.5663
6	14.086	2.2535	2.2738	0.9683	0.5748	0.4842
7	14.435	2.1365	2.6191	1.1541	0.6404	0.5551
8	13.907	2.1308	2.4347	0.8822	0.6214	0.4738
9	14.193	2.1781	2.3821	1.1799	0.6078	0.5643
10	14.194	2.1242	2.5606	0.9538	0.6212	0.5107
11	14.137	2.2028	2.3770	1.1336	0.6034	0.5328
12	14.238	2.1595	2.4696	1.0355	0.6358	0.5195

that the final result is not very sensitive to small changes of the values a_∞ and b_∞. Oscillations of a_n and b_n around the limiting values (see Table 3) are responsible for the subtleties of the spectrum. The more levels of the continued fraction is taken into consideration, the more details of the spectrum one is able to get.

We have applied the above methods to calculate the spectral density ρ for three primitive cubic lattices. The results are discussed in the next section.

5. Results

The spectra obtained by the use of the RS, LA and CF methods are given in Figs. 1–3. First, we compare efficiencies and accuracies of the methods.

In the case of RS and LA techniques, a good estimate of the accuracy is the so-called computational resolution (see [17,18]) defined as

$$N_\lambda = \frac{\lambda_{max} - \lambda_{min}}{\Delta\lambda}\,, \tag{46}$$

where $\lambda_{max} - \lambda_{min}$ is the range of λ values and $\Delta\lambda$ is the resolution.

It can be shown [18] that the relative error of the amplitude of the spectrum $\delta\rho/\rho$ is closely related to N_λ. In fact, for values of λ that are not too close to critical points of the spectra (see next section), $\delta\rho/\rho$ is proportional to N_λ^{-1}. In the vicinity of highly peaked critical points the error becomes somewhat larger.

In the RS method we found the eigenvalues of $\hat{T}(\mathbf{k})$ for about 12 000 points in IBZ. N_λ was equal to 300 and $\delta\rho/\rho \approx 1\%$.

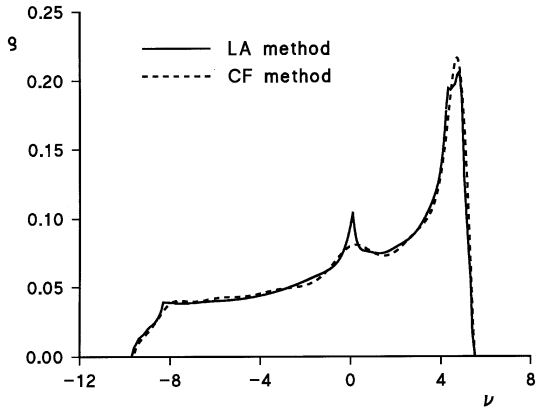

Fig. 1. The spectral density $\rho(v)$ for the sc lattice. The solid curve denotes the spectrum obtained by the use of the LA method and the dotted one was calculated by the CF method. The results of the RS method are indistinguishable from those of the LA on the scale of the figure.

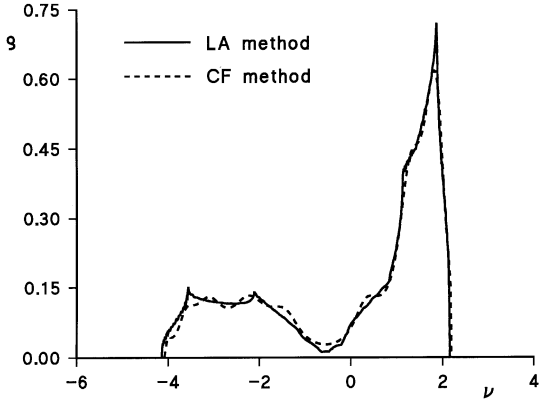

Fig. 2. Same as in Fig.1 for the fcc lattice.

In the LA method calculations we found $\lambda_i(\mathbf{k})$ and $\nabla\lambda_i(\mathbf{k})$ for about 3000 points in IBZ, obtaining $N_\lambda = 2800$ and the accuracy $\delta\rho/\rho \approx 0.2\%$. The ratio of computing times for both the methods is $T_{RS}/T_{LA} \approx 1.8$.

The above values are a direct evidence that the LA method is more effective and, at the same time, less time consuming from the two.

Let us now consider the CF method. To compute the integrals (42) we used 12 000 values of $\mathbf{k}$. The total computing time $T_{CF}/T_{RS} \approx 1.1$ and the accuracy was equal to $\delta\rho/\rho \approx 1.5\%$ (again the above holds for the points not too close to the singularities of the spectrum – in the vicinity of which the error $\delta\rho/\rho$ may even come up to 4%). The CF method gives us quickly quite a good approximation of a spectrum – to obtain the above-described results we took only 7 levels of the continued fraction (43). However,

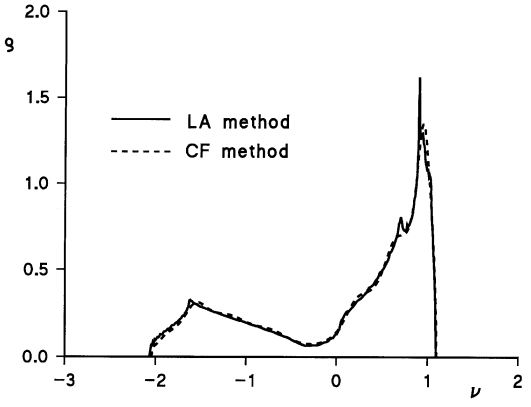

Fig. 3. Same as in Fig.1 for the bcc lattice.

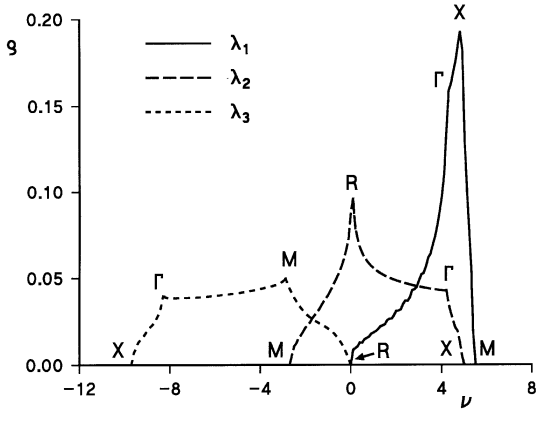

Fig. 4. Contributions to the spectrum coming from different eigenvalues λ_i for the sc lattice. The eigenvalues λ_1 and λ_2 correspond to the transversal polarization modes whereas λ_3 to the longitudinal one. The letters denote the critical points as described in Table 4.

as the crystal spectrum is not analytical, to render all the subtle details of it one would have to take a very large number of the continued fraction levels. It is worth mentioning that the CF method is well-suited to deal with the fluid spectra which are much more smoother than the solid one and contains no critical points.

Figs. 4–6 present the contributions to the spectrum $\rho(\nu)$ coming from the different eigenvalues $\lambda_i(\mathbf{k})$. Here also we mark the van Hove singularities of the spectra, i.e. points of discontinuity of the first derivative of $\rho(\nu)$. There are several kinds of singularities appearing in these spectra: analytical critical points (coming from those points in $\mathbf{k}$ space where $\nabla\lambda_i(\mathbf{k})=0$), singular critical points (corresponding to the discontinuities in $\nabla\lambda_i(\mathbf{k})$), fluted critical points (caused by the degeneracies of eigenvalues $\lambda_i(\mathbf{k})$ in the high-symmetry points of the Brillouin zone) [15,19,20]. Moreover, there are also some non-analytical critical points due to the long-range interactions in the

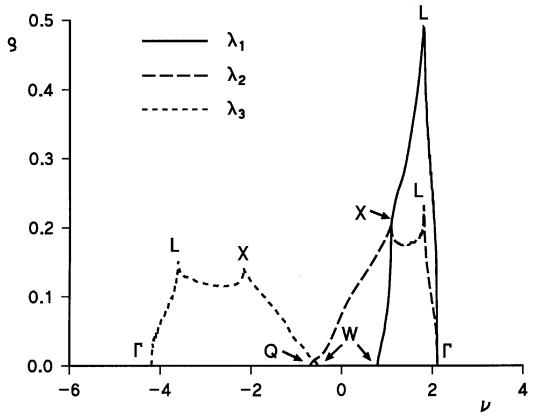

Fig. 5. Same as in Fig. 4 for fcc lattice. The letters denote the critical points as described in Table 5.

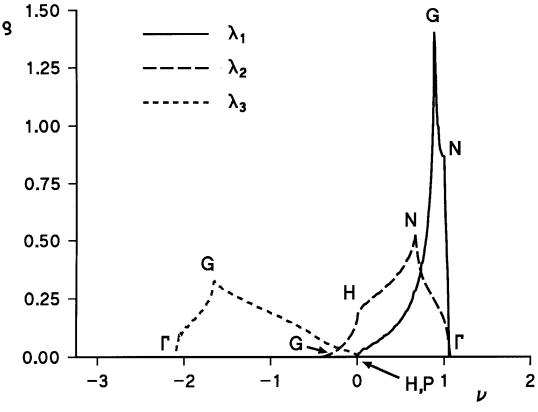

Fig. 6. Same as in Fig. 4 for bcc lattice. The letters denote the critical points as described in Table 6.

system [20–22]. We have identified all the critical points in the spectra, found the **k** values to which they correspond and checked the Morse relations [19,20] for them. The results of this analysis are given in Tables 4–6, where we list the critical points, their position in the **k** space and their topological indexes (we apply here a standard notation [15] with index 0 designating minimum, 3-maximum, whereas 1 and 2 stand for two kinds of saddle points).

It is worth paying attention to the overall structure of the spectrum. We see that the contributions coming from the longitudinal (corresponding to the eigenvalue λ_3) and transverse (corresponding to λ_1 and λ_2) modes are rather separated (especially in case of fcc and bcc crystals) so that the spectrum has a characteristic two-peaked structure.

Table 4
The critical points for the contributions to the spectral density from the eigenvalues λ_i, $i = 1, 2, 3$ for the sc lattice

Eigenvalue	Label	Coordinates $(1/2\pi)(k_x, k_y, k_z)$	Topological index
λ_1	Γ	$(0, 0, 0)$	1
	X	$(\frac{1}{2}, 0, 0)$	2
	M	$(\frac{1}{2}, \frac{1}{2}, 0)$	3
	R	$(\frac{1}{2}, \frac{1}{2}, \frac{1}{2})$	0
λ_2	Γ	$(0, 0, 0)$	2
	X	$(\frac{1}{2}, 0, 0)$	3
	M	$(\frac{1}{2}, \frac{1}{2}, 0)$	0
	R	$(\frac{1}{2}, \frac{1}{2}, \frac{1}{2})$	1
λ_3	Γ	$(0, 0, 0)$	2
	X	$(\frac{1}{2}, 0, 0)$	0
	M	$(\frac{1}{2}, \frac{1}{2}, 0)$	1
	R	$(\frac{1}{2}, \frac{1}{2}, \frac{1}{2})$	3

Table 5
Same as in Table 4 but for the fcc lattice; (s) – stands for the singular critical point and (*) denotes a singular point producing the discontinuities only in the higher derivatives of $\rho(\lambda)$ (imperceptible in the $\rho(\lambda)$ spectrum)

Eigenvalue	Label	Coordinates $(1/2\pi)(k_x, k_y, k_z)$	Topological index
λ_1	Γ	$(0, 0, 0)$	3
	X	$(\frac{1}{2}, 0, 0)$	1
	W	$(\frac{1}{2}, \frac{1}{4}, 0)$	0
	L	$(\frac{1}{4}, \frac{1}{4}, \frac{1}{4})$	2
λ_2	Γ	$(0, 0, 0)$	3
	X	$(\frac{1}{2}, 0, 0)$	2
	W*	$(\frac{1}{2}, \frac{1}{4}, 0)$	1(s)
	L	$(\frac{1}{4}, \frac{1}{4}, \frac{1}{4})$	2
	Q	$\approx(0.34, 0.34, 0)$	0(s)
λ_3	Γ	$(0, 0, 0)$	0
	X	$(\frac{1}{2}, 0, 0)$	1
	W	$(\frac{1}{2}, \frac{1}{4}, 0)$	3(s)
	L	$(\frac{1}{4}, \frac{1}{4}, \frac{1}{4})$	1
	Q*	$\approx(0.34, 0.34, 0)$	2(s)

Table 6
Same as in Table 5 but for the bcc lattice; (**) denotes a singular point giving rise to the discontinuities only in the second derivative of $\rho(\lambda)$

Eigenvalue	Label	Coordinates $(1/2\pi)(k_x, k_y, k_z)$	Topological index
λ_1	Γ	$(0,0,0)$	3
	N	$(\frac{1}{4}, \frac{1}{4}, 0)$	2
	H	$(\frac{1}{2}, 0, 0)$	0
	P	$(\frac{1}{4}, \frac{1}{4}, \frac{1}{4})$	0(s)
	G	$\approx(0.34, 0.16, 0.16)$	1
λ_2	Γ	$(0,0,0)$	3
	N	$(\frac{1}{4}, \frac{1}{4}, 0)$	2
	H	$(\frac{1}{2}, 0, 0)$	1
	P*	$(\frac{1}{4}, \frac{1}{4}, \frac{1}{4})$	1(s)
	G**	$\approx(0.34, 0.16, 0.16)$	0(s)
λ_3	Γ	$(0,0,0)$	0
	N	$(\frac{1}{4}, \frac{1}{4}, 0)$	1
	H	$(\frac{1}{2}, 0, 0)$	3
	P	$(\frac{1}{4}, \frac{1}{4}, \frac{1}{4})$	3(s)
	G*	$\approx(0.34, 0.16, 0.16)$	2(s)

6. Comparison with computer simulation data for fluids

In this section we compare the calculated $\rho(v)$ spectra for the cubic lattice with the analogous spectra for the hard-sphere fluid. Computer simulations for such a fluid were performed by Cichocki and Felderhof [3]. They considered the system of spheres distributed according to the equilibrium statistics. Each sphere had in its center a polarizable dipole with polarizability α. They calculated the successive moments of the spectra for a given configuration of particles and then averaged over a large number of configurations. In this way, they got the coefficients c_n in the power series (41) and, finally, used the CF method to obtain the spectral density (in the case of a fluid, the reciprocal space techniques cannot be applied because of the lack of periodicity). The simulations have been run at six different values of the volume fraction Φ between $\Phi = 0.1$ (semi-diluted fluid) and $\Phi = 0.5$ (very dense fluid); Φ is the ratio of the volume occupied by spheres to the total volume. Fig. 7 shows the results for spectral density $\rho' = \rho n$ as a function of $v' = v/n$, where n is the number density. Note that after such a rescaling, the fluid spectrum tends to the universal lineshape in the low-density limit [10].

In Fig. 8 we present the comparison of the spectrum for a very dense fluid ($\Phi = 0.5$) with the rescaled spectrum of the bcc crystal. We see that the $\rho'(v')$ spectrum for the crystal lattice is modeling the behavior of ρ' for the dense fluid in quite a good way. An analogous plot for fcc lattice is qualitatively similar. Of course, in the fluid spectrum

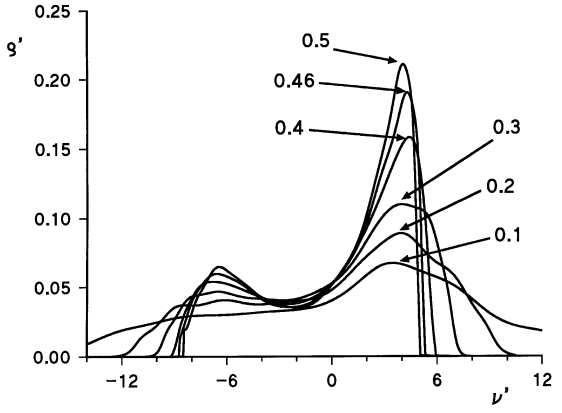

Fig. 7. The rescaled spectral density $\rho'(\nu')$ for the hard sphere fluid for the volume fractions $\Phi = 0.1, 0.2, 0.3, 0.4, 0.46, 0.5$.

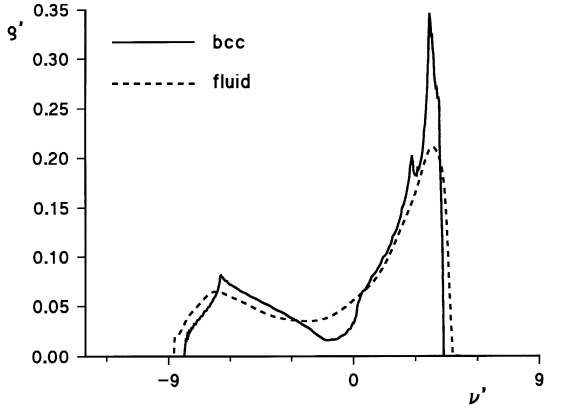

Fig. 8. The rescaled spectral density $\rho'(\nu')$ for the dense hard sphere fluid ($\Phi = 0.5$) and for the bcc lattice.

we will not find van Hove's singularities (again because of the lack of periodicity). That is why there are no sharp peaks in the fluid spectrum and, on the whole, it is much more smooth than the solid one. The structure, however, remains the same. In particular, one can find the characteristic two broad peaks in the fluid spectrum the counterparts of which for the solid are connected with the longitudinal and transverse polarizability modes.

What is even more interesting is that this two-peaked structure survives also in the diluted fluid – the traces of it can be seen in Fig. 7 even for the $\Phi = 0.1$! We observe here that, although the spectrum broadens and smoothes down as the density of fluid decreases, the overall structure remains the same. Therefore, it seems that even for the low densities the fluid "feels" in a way the transverse and longitudinal polarization modes.

It is worth pointing out that this structure was so far not described analytically. The approximate analytical expression for $\rho(v)$ derived by Cichocki and Felderhof [10] in the low-density limit does not show the above-mentioned two-peak structure. The problem seems to be that in the fluid one cannot decompose $\rho(v)$ into the contributions coming from the respective eigenvalues of $\hat{T}(\mathbf{k})$. Instead one performs an average over configurations which does not favor any direction in space. Hence simple approximations lead in a "natural way" to one-peak structure.

7. Conclusions

We have found the electrostatic spectra of renormalized polarizability for the nonpolar dielectric with cubic crystal structure. Three methods (RS, LA and CF) have been applied to compute the spectrum. It has been found that a very simple continued fraction method gives very good results. We have analyzed the obtained spectra and identified their critical points. Next, we have shown that the structure of the spectra for a fluid corresponds in a wide range of density to the solid spectra with the transverse and longitudinal modes. This fact must be taken into account if one wants to describe Drude–Lorentz fluid spectra in a proper way.

References

[1] M.J. Renne, B.R.A. Nijboer, Chem. Phys. Lett. 1 (1967) 317.
[2] L. Onsager, J. Am. Chem. Soc. 58 (1936) 1486.
[3] B. Cichocki, B.U. Felderhof, J. Chem. Phys. 92 (1990) 6104.
[4] Z. Chen, R.M. Stratt, J. Chem. Phys. 95 (1991) 2669.
[5] G. Seeley, T. Keyes, J. Chem. Phys. 91 (1989) 5581.
[6] B.Cichocki, B.U. Felderhof, J. Chem. Phys. 92 (1990) 6112.
[7] B. Cichocki, B.U. Felderhof, J. Chem. Phys. 90 (1989) 4960.
[8] J.A. Leegwater, S. Mukamel, J. Chem. Phys. 99 (1993) 6062.
[9] J.A. Leegwater, S. Mukamel, Phys. Rev. A 49 (1994) 146.
[10] B. Cichocki, B.U. Felderhof, J. Chem. Phys. 104 (1996) 3013.
[11] B. Cichocki, B.U. Felderhof, J. Chem. Phys. 107 (1997) 6390.
[12] H.S. Wall, Analytic Theory of Continued Fractions, Van Nostrand, Princeton, 1948.
[13] W.B. Jones, W.J. Thorn, Continued Fractions – Analytic Theory and Applications, in Encyclopedia of Mathematics and its Applications 11, Addison-Wesley, Reading, MA, 1980.
[14] A.A. Lucas, Physica 35 (1967) 353.
[15] L. van Hove, Phys. Rev. 89 (1953) 1189.
[16] B.R.A. Nijboer, F.W. de Wette, Physica 23 (1957) 309.
[17] G. Gilat, Methods Comput. Phys. 15 (1976) 317.
[18] G. Gilat, J. Comp. Phys. 10 (1972) 432.
[19] J.C. Philips, Phys. Rev. 104 (1956) 1263.
[20] A.A. Maradudin, E.W. Montroll, G.H. Weiss, Solid State Phys. (Suppl.) 3 (1963).
[21] H.R. Rosenstock, Phys. Rev. 111 (1958) 755.
[22] M. Smollett, Proc. Phys. Soc. (London) A 65 (1952) 109.